

This document is the accepted manuscript version of the following article:

Pudza, I., Bocharov, D., Anspoks, A., Krack, M., Kalinko, A., Welter, E., & Kuzmin, A. (2023). Unraveling the interlayer and intralayer coupling in two-dimensional layered MoS<sub>2</sub> by X-ray absorption spectroscopy and ab initio molecular dynamics simulations. *Materials Today Communications*, 35, 106359 (8 pp.).  
<https://doi.org/10.1016/j.mtcomm.2023.106359>

# Unraveling the interlayer and intralayer coupling in two-dimensional layered MoS<sub>2</sub> by X-ray absorption spectroscopy and ab initio molecular dynamics simulations

Inga Pudza<sup>a</sup>, Dmitry Bocharov<sup>a,\*</sup>, Andris Anspoks<sup>a</sup>, Matthias Krack<sup>b</sup>, Aleksandr Kalinko<sup>c,a</sup>, Edmund Welter<sup>c</sup>, Alexei Kuzmin<sup>a,\*\*</sup>

<sup>a</sup>*Institute of Solid State Physics, University of Latvia, Kengaraga street 8, LV-1063 Riga, Latvia*

<sup>b</sup>*Paul Scherrer Institute, Villigen CH-5232, Switzerland*

<sup>c</sup>*Deutsches Elektronen-Synchrotron DESY, Notkestr. 85, 22607 Hamburg, Germany*

---

## Abstract

Understanding interlayer and intralayer coupling in two-dimensional layered materials (2DLMs) has fundamental and technological importance for their large-scale production, engineering heterostructures, and development of flexible and transparent electronics. At the same time, the quantification of weak interlayer interactions in 2DMLs is a challenging task, especially, from the experimental point of view. Herein, we demonstrate that the use of X-ray absorption spectroscopy in combination with reverse Monte Carlo (RMC) and ab initio molecular dynamics (AIMD) simulations can provide useful

---

\*Corresponding author

\*\*Corresponding author

*Email addresses:* [inga.pudza@cfi.lu.lv](mailto:inga.pudza@cfi.lu.lv) (Inga Pudza), [bocharov@cfi.lu.lv](mailto:bocharov@cfi.lu.lv) (Dmitry Bocharov), [andris.anspoks@cfi.lu.lv](mailto:andris.anspoks@cfi.lu.lv) (Andris Anspoks), [matthias.krack@psi.ch](mailto:matthias.krack@psi.ch) (Matthias Krack), [aleksandr.kalinko@desy.de](mailto:aleksandr.kalinko@desy.de) (Aleksandr Kalinko), [edmund.welter@desy.de](mailto:edmund.welter@desy.de) (Edmund Welter), [a.kuzmin@cfi.lu.lv](mailto:a.kuzmin@cfi.lu.lv) (Alexei Kuzmin)

*Preprint submitted to Materials Today Communications*

*June 19, 2023*

information on both interlayer and intralayer coupling in 2DLM 2H<sub>c</sub>-MoS<sub>2</sub>. The analysis of the low-temperature (10-300 K) Mo K-edge extended X-ray absorption fine structure (EXAFS) using RMC simulations allows for obtaining information on the means-squared relative displacements  $\sigma^2$  for nearest and distant Mo-S and Mo-Mo atom pairs. This information allowed us further to determine the strength of the interlayer and intralayer interactions in terms of the characteristic Einstein frequencies  $\omega_E$  and the effective force constants  $\kappa$  for the nearest ten coordination shells around molybdenum. The studied temperature range was extended up to 1200 K employing AIMD simulations which were validated at 300 K using the EXAFS data. Both RMC and AIMD results provide evidence of the reduction of correlation in thermal motion between distant atoms and suggest strong anisotropy of atom thermal vibrations within the plane of the layers and in the orthogonal direction.

*Keywords:* 2D layered materials, interlayer coupling, extended X-ray absorption fine structure, reverse Monte Carlo simulations, ab initio molecular dynamics

---

## 1. Introduction

The field of 2D layered materials (2DLMs) is a rapidly growing area of material science, offering significant potential for technological advancements [1, 2]. During the last decades, 2DLMs have generated significant interest due to their extraordinary electronic, magnetic, optical, catalytic, transport, and tribological properties [3, 4, 5, 6, 7, 8, 9]. The 2DLM family encompasses a range of substances, including transition-metal dichalcogenides, 2D oxides and hydroxides, boron nitride, and single-element compounds like silicene, phosphorene, germanene, and graphene [1, 5, 10]. The unique structure of 2DLMs is determined by strong in-plane (intralayer) covalent bonding and weak out-of-plane (interlayer) van-der-Waals (vdW) interactions.

The strength of the interlayer coupling plays a crucial role in the process of exfoliating thin layers and assembling van-der-Waals heterostructures, which is vital for engineering the electronic, optical, and mechanical properties of 2DLMs for their use in devices [11, 12, 13]. Therefore, accurate quantification of this weak interlayer coupling has fundamental, theoretical, and technological implications for 2DLMs large-scale production and the ongoing development of flexible and transparent electronics that utilize these materials. For instance, the insertion of an atomic layer-deposited  $\text{TiO}_2$  interlayer between exfoliated  $\text{MoS}_2$  and an electrode can improve the performance of  $\text{MoS}_2$  photodetectors [14]. At the same time, encapsulating  $\text{MoS}_2$  layers with hexagonal boron nitride in low-power transistors offers protection from environmental factors and ensures stability in device operation, even at elevated temperatures [15]. Furthermore, future integrated circuits will utilize transistors based on 2D semiconductors that are coupled through van-der-Waals

interactions with high- $\kappa$  dielectric and metal contacts [16, 17]. A microprocessor based on an active channel material made of molybdenum disulfide was demonstrated [18, 19] and opens up new opportunities for next-generation low-power electronics [20].

Although the physical and chemical properties of 2DLMs associated with the intralayer bonding have been studied both experimentally and theoretically [1, 11, 12], the extensive atomic and nanoscale characteristics of their interlayer vdW-dependent properties (for example, enhanced in-plane stiffness, band gap opening, band structure, and carrier mobility engineering, interlayer charge transfer/distribution, etc.) is still a major challenge due to the highly anisotropic nature of the weak interlayer interactions, the lack of accurate experimental methods to quantify such complex interlayer behavior, and complexity of manipulations with ultra-thin and highly transparent 2DLMs. Therefore, gaining a deeper insight into the weak interlayer interactions in 2D layered materials and their interactions with different substrates is critical for improving the transfer efficiency and uniform thickness of printed flakes. This, in turn, is important for the production of high-quality, large-scale 2DLM-based devices at the micro- and nanoscale [21, 22, 23, 24].

Until now, the experimental approaches for detecting interlayer coupling in 2DLMs have been limited to photoluminescence, Raman, and angle-resolved photoemission spectroscopy [12]. However, these methods do not give direct information on the atomic structure of the material [25]. Note also that Raman spectroscopy is a selective method providing information about the frequency of vibrations but not their amplitude. Theoretical modeling of vdW interactions is also a difficult task because of its highly non-local na-

ture, so this contribution is often accounted for a *posteriori* [26].

The present study is largely based on the use of X-ray absorption spectroscopy (XAS) which is a direct local structural tool complementary to diffraction. The technique has been employed in the past to probe the short-range order in 2DLMs [27, 28, 29]. However, the conventional approach to the data analysis of the X-ray absorption spectrum, based on multi-shell modeling, cannot provide reliable information on the medium-range (across the vdW spacing) interlayer interactions due to a strong correlation between model parameters for distant coordination shells during fitting [30, 31]. At the same time, the extraction of such information should be in principle possible since the range of atomic structure around the absorbing atoms probed by XAS extends often up to 10–15 Å as follows from the calculations of the photoelectron mean-free path [30, 31]. Nevertheless, this task is challenging and requires the combined use of advanced theoretical methods and high-quality experimental data, i.e. the extended X-ray absorption fine structure (EXAFS) spectra, which can be recorded nowadays at last-generation synchrotron radiation sources. Recent developments in the EXAFS data analysis include two approaches based on atomistic simulations – reverse Monte Carlo (RMC) and molecular dynamics (MD) methods [31]. Both approaches enable precise examination of the local atomic structure and lattice dynamics with high accuracy taking into account multiple-scattering contributions [32] and are well suited for the analysis of distant coordination shells, for example, interactions between atoms located in neighbouring layers of 2DLMs. Note that a number of previous works dedicated to the EXAFS studies of MoS<sub>2</sub> utilized conventional approach, i.e., the multi-shell fitting, and were limited

to the analysis of the first two coordination shells of molybdenum atoms only [27, 28, 33, 34, 35, 36, 37].

In this study, a complex approach based on X-ray absorption spectroscopy, ab initio molecular dynamics (AIMD), and reverse Monte Carlo methods was employed to provide insights into the local dynamics in 2DLM  $2H_c$ -MoS<sub>2</sub>. We demonstrated, for the first time, the possibility of extracting the temperature dependence (10-300 K) of intralayer and interlayer interactions in 2DLM  $2H_c$ -MoS<sub>2</sub> for the nearest ten coordination shells around molybdenum atoms. This information was obtained through the analysis of the Mo K-edge EXAFS spectra using the reverse Monte Carlo method. The low-temperature experimental results were complemented with high-temperature (300-1200 K) AIMD simulations, which were validated at 300 K using EXAFS data. Both approaches allowed us to observe similar trends in the lattice dynamics of  $2H_c$ -MoS<sub>2</sub> and to distinguish between interlayer and intralayer interactions.

## 2. Experimental

Commercial molybdenum(IV) sulfide (MoS<sub>2</sub>) powder (Sigma-Aldrich, 98%) was used in all experiments. The phase of the sample was confirmed using X-ray powder diffraction and Raman spectroscopy.

The X-ray absorption experiments were conducted at the Mo K-edge as a function of temperature from 10 to 300 K at the DESY PETRA-III P65 beamline [38]. The storage ring was operating at  $E=6.08$  GeV and current  $I=100$  mA in top-up 480 bunch mode. A fixed exit double-crystal Si(311) monochromator was used, and the harmonic rejection was achieved by the Rh-coated silicon plane mirror. The X-ray absorption spectra were recorded

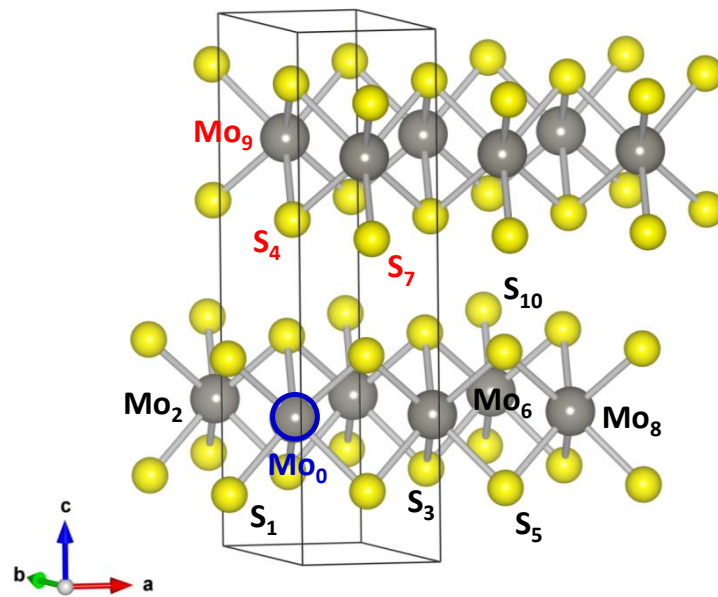


Figure 1: Crystallographic structure of 2H<sub>c</sub>-MoS<sub>2</sub>. Atoms located in the nearest ten coordination shells around the Mo<sub>0</sub> atom are indicated.

in transmission mode using two ionization chambers, while the temperature was controlled using a liquid helium flow cryostat.

The sample was prepared by mixing MoS<sub>2</sub> powder with cellulose in an agate mortar and pressing the mixture into a pellet using a hydraulic press. Its thickness was optimized to get the value of the absorption edge jump  $\Delta\mu=1$ . The Mo K-edge EXAFS spectra were extracted following the conventional procedure [30]. The Fourier transforms (FTs) of the EXAFS spectra were calculated using 10% Gaussian function. Note that the peak positions in all FTs differ from their true crystallographic values because of the EXAFS phase shifts.

### 3. Reverse Monte-Carlo simulations

The structural information encoded in the experimental Mo K-edge EXAFS spectra was extracted using the reverse Monte-Carlo method based on an evolutionary algorithm approach (RMC/EA) [39, 40]. The simulations were performed by the EvAX code [40]. The RMC/EA method involves randomly changing the atomic coordinates within a three-dimensional structure model of the material in order to minimize the difference between the experimental and calculated configuration-averaged EXAFS spectra. Both structural and thermal disorder in the material, as well as multiple-scattering effects, were taken into account.

The initial structural models for the RMC/EA calculations were constructed based on diffraction data (2H<sub>c</sub>-MoS<sub>2</sub>, space group  $P6_3/mmc$  (194),  $a=b=3.160$  Å,  $c=12.295$  Å [41]) in the form of the supercell ( $4a\times 4b\times 4c$ ) containing 384 atoms. The atoms in the supercell were randomly displaced



at each iteration with the maximum allowed displacement of 0.4 Å. The configuration-averaged EXAFS spectra at the Mo K-edge were calculated using the *ab initio* self-consistent real-space multiple-scattering (MS) FEFF8.5L code [32, 42] taking into account multiple-scattering contributions up to the 5<sup>th</sup> order. The complex energy-dependent exchange-correlation Hedin-Lundqvist potential was employed to account for inelastic effects [43]. The amplitude scaling parameter  $S_0^2$  was set to 1.

The experimental and calculated Mo K-edge EXAFS spectra were compared in both the direct ( $R$ ) and reciprocal ( $k$ ) space utilizing the Morlet wavelet transforms [44]. The fitting was done in the  $k$ -space range from 2.2 Å<sup>-1</sup> to 18.3 Å<sup>-1</sup> and the  $R$ -space range from 1.1 Å to 6.3 Å. The convergence of each RMC simulation was achieved after 4000 iterations. The RMC/EA calculations were performed for 32 atomic configurations simultaneously. At least three RMC/EA simulations were conducted for each experimental data set, using different sequences of pseudo-random numbers. The configuration-averaged EXAFS spectra agree well with the experimental data at all temperatures supporting the reliability of the obtained structural models.

Atomic coordinates were used to calculate radial distribution functions (RDFs) and estimate structural parameters of interest. The means-square relative displacement factors  $\sigma^2$  for Mo–S and Mo–Mo atom pairs were calculated using the median absolute deviation (MAD) method [45, 46].

#### 4. Ab initio molecular dynamics

Ab initio molecular dynamics (AIMD) simulations were based on Kohn-Sham density functional theory (DFT) [47] and were performed in the NVT ensemble at four different temperatures (300 K, 600 K, 900 K, and 1200 K) using the CP2K code [48]. The code employs a localized basis set of Gaussian-type orbital functions for the description of the Kohn-Sham matrix within the framework of the Gaussian Plane Waves method [49, 50]. We used PBE exchange-correlation functional [51] with Grimme correction [52].

Preliminary structure DFT calculations with full optimization of geometry gave the lattice constants of bulk  $2H_c$ -MoS<sub>2</sub> equal to  $a_0 = 3.164$  Å and  $c_0 = 12.199$  Å. Orthorhombic supercell  $6a_0 \times 4a_0 \times 2c_0$  with 576 atoms (192 Mo atoms and 384 S atoms) was used for AIMD calculations. The size of the supercell was equal to  $18.986$  Å  $\times$   $21.923$  Å  $\times$   $24.398$  Å. CSVN (Canonical Sampling through Velocity Rescaling) thermostat [53] was used in the calculations. The system was first equilibrated for 15 ps, followed by a production run of 30 ps. The time step was  $\Delta t = 0.5$  fs. A set of at least 4000 atomic configurations was recorded during the production run and further used for the calculation of the configuration-averaged EXAFS spectrum by the MD-EXAFS approach [30, 54]. The AIMD results calculated at different temperatures were used to obtain temperature-dependence of the means-square relative displacement factors  $\sigma^2$  for required Mo-S and Mo-Mo interatomic distances.

## 5. Results and discussion

The crystallographic structure of 2DLM 2H<sub>c</sub>-MoS<sub>2</sub> with hexagonal symmetry is shown in Figure 1 [55]. Molybdenum atoms have trigonal prismatic coordination and are covalently bonded to six sulfur ions. The MoS<sub>6</sub> units form two layers per unit cell which are held together along the *c*-axis by weak vdW interactions. The interlayer gap is about 3 Å. In Figure 1, the Mo and S atoms located in the nearest ten coordination shells around the absorbing molybdenum atom (Mo<sub>0</sub>) are labeled. Note that three shells including sulfur (two S<sub>4</sub> and twelve S<sub>7</sub>) and molybdenum (six Mo<sub>9</sub>) atoms belong to the nearest neighboring layers, therefore, their analysis can provide original information on the interlayer interactions.

The values of Mo–S and Mo–Mo interatomic distances for the first ten coordination shells in 2H<sub>c</sub>-MoS<sub>2</sub> are reported in Table 1. As can be seen, the atoms (S<sub>4</sub>, S<sub>7</sub>, and Mo<sub>9</sub>) located in the nearest neighboring layers and being the closest to the absorbing molybdenum (Mo<sub>0</sub>) belong to its distant coordination shells with large interatomic distances. Nevertheless, these atoms should contribute to EXAFS spectra as can be estimated from the value of the mean-free path of the excited 1s(Mo) photoelectron (see, the inset in Figure 2).

The Mo K-edge EXAFS spectra of 2H<sub>c</sub>-MoS<sub>2</sub> and their FTs are dominated at all studied temperatures in the range of 10-300 K by a contribution from the first two coordination shells, which are composed of six sulfur (S<sub>2</sub>) and six molybdenum (Mo<sub>2</sub>) atoms (Figure 2). However, several structural peaks are well visible in FTs above 3.2 Å up to at least 10 Å. Their small amplitude compared to that of the first two peaks at 2.0 and 2.9 Å is caused

by the overlap of shells, thermal disorder, and interference effects between single-scattering and high-order multiple-scattering contributions in EXAFS spectra. In particular, the effect of thermal disorder is clearly seen upon increasing temperature as the EXAFS spectra damping at high- $k$  values or a reduction of the peak amplitude in FTs. While the reliable analysis of distant shells is challenging within the conventional methodology, it can be reliably performed using the reverse Monte Carlo method [40, 56, 57, 58].

Table 1: Values of Mo-S and Mo-Mo interatomic distances for the first ten coordination shells of molybdenum calculated from the crystallographic structure of  $2H_c$ -MoS<sub>2</sub> [55]. Interlayer distances are given in bold. The values of characteristic Einstein frequencies ( $\omega_E$ ) and the effective force constants ( $\kappa$ ) obtained from the RMC analysis are also given.

Atom pair	Distance (Å)	$\omega_E$ (THz)	$\kappa$ (N/m)
Mo <sub>0</sub> -S <sub>1</sub>	2.37	62±3	152±13
Mo <sub>0</sub> -Mo <sub>2</sub>	3.16	44±2	152±13
Mo <sub>0</sub> -S <sub>3</sub>	3.95	38±2	56±5
<b>Mo<sub>0</sub>-S<sub>4</sub></b>	<b>4.64</b>	<b>26±2</b>	<b>26±5</b>
Mo <sub>0</sub> -S <sub>5</sub>	5.06	40±2	65±5
Mo <sub>0</sub> -Mo <sub>6</sub>	5.48	34±2	94±5
<b>Mo<sub>0</sub>-S<sub>7</sub></b>	<b>5.62</b>	<b>36±2</b>	<b>51±5</b>
Mo <sub>0</sub> -Mo <sub>8</sub>	6.32	34±2	93±6
<b>Mo<sub>0</sub>-Mo<sub>9</sub></b>	<b>6.41</b>	<b>18±2</b>	<b>25±5</b>
Mo <sub>0</sub> -S <sub>10</sub>	6.75	37±2	55±5

Examples of the RMC simulations of the Mo K-edge EXAFS spectra for  $2H_c$ -MoS<sub>2</sub> at two selected temperatures (10 and 300 K) are shown in Figure 3 in  $k$ -space,  $R$ -space, and wavelet( $k, R$ )-space. The theory reproduces well

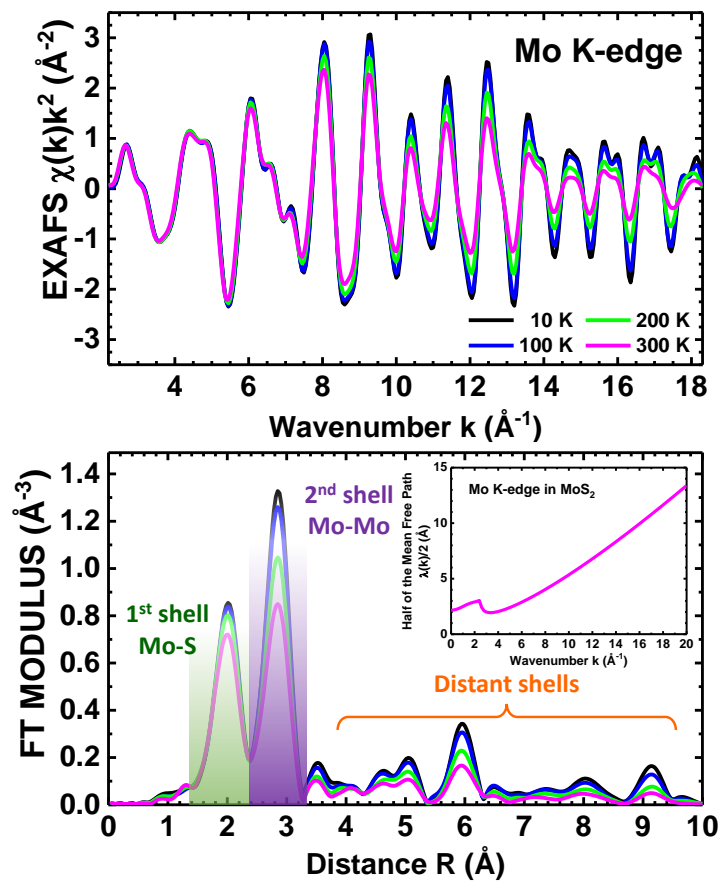


Figure 2: Temperature-dependent Mo K-edge EXAFS spectra  $\chi(k)k^2$  and their Fourier transforms for 2H<sub>c</sub>-MoS<sub>2</sub>. The calculated half of the mean free path of the photoelectron is shown in the inset and explains the presence of distant coordination shells.

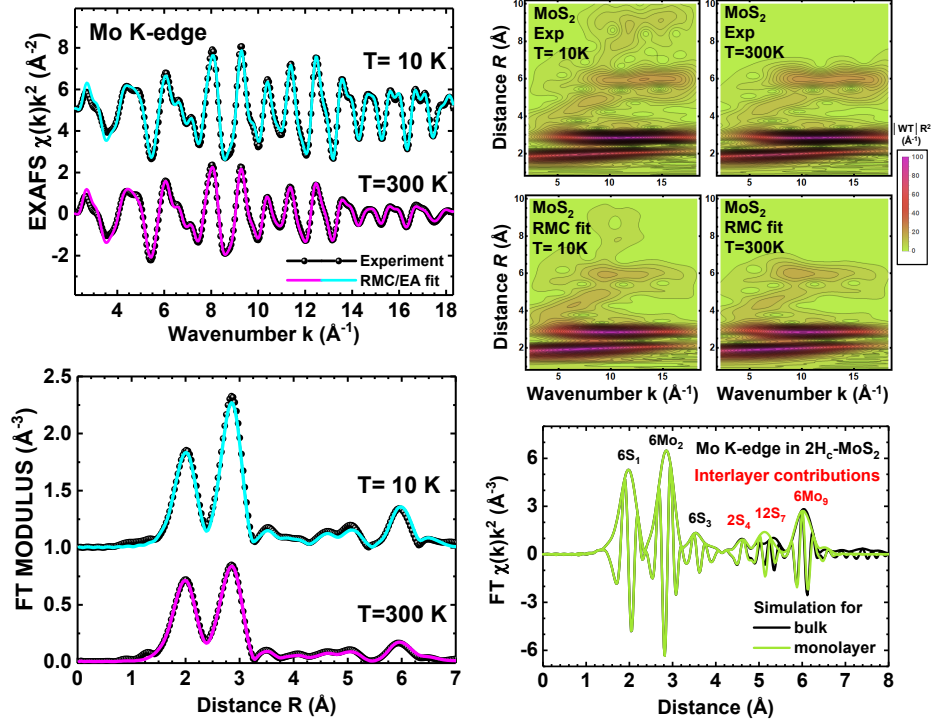


Figure 3: Results of RMC calculations for the Mo K-edge in  $2H_c$ - $\text{MoS}_2$  at 10 K and 300 K. The EXAFS spectra  $\chi(k)k^2$  and their Fourier transforms are shown in the left panels. Wavelet transforms of EXAFS spectra are shown in the upper right panel. A comparison between the calculated Fourier transforms for the bulk and single monolayer  $\text{MoS}_2$  is shown in the lower right panel.

the experimental data, allowing for a detailed analysis of thermal disorder effects within the coordination shells up to 7 Å.

To estimate the contribution of atoms from the nearest neighboring layers to the total EXAFS spectrum, the Mo K-edge EXAFS spectra of bulk and single monolayer  $\text{MoS}_2$  were additionally calculated using the crystallographic structure of  $2H_c$ - $\text{MoS}_2$  [55], without considering thermal disorder. Their FTs are compared in the lower right panel in Figure 3. As one can see,

the main difference between the two FTs is observed between 4.2 and 6.5 Å, where the interlayer contributions appear. At the same time, their effect is rather small and requires a delicate treatment during analysis.

The coordinates of atoms obtained in the RMC simulations were used to compute the radial distribution functions (RDFs)  $g(R)$  and the means-square relative displacements (MSRDs)  $\sigma^2$  at each temperature (Figure 3). The temperature dependencies (10-300 K) of the obtained MSRDs  $\sigma^2(T)$  were further approximated by the correlated Einstein model [59]. As a result, the characteristic Einstein frequencies  $\omega_E$  and the effective force constants  $\kappa$  were obtained for all coordination shells and are reported in Table 1 and Figure 4. The relationship between the two parameters is  $\omega_E = \sqrt{\kappa/\mu}$ , where  $\mu$  is the reduced mass of an atom pair. The largest value of the Einstein frequency,  $\omega_E = 62$  THz, was found for the Mo<sub>0</sub>-S<sub>1</sub> bonds in the first coordination shell due to strong covalent bonding between the nearest Mo and S atoms. The effective force constant  $\kappa = 152 \pm 13$  N/m for the Mo<sub>0</sub>-S<sub>1</sub> bonds can be compared to the one (194 N/m) estimated from the internal Raman E<sub>2g</sub><sup>1</sup> mode at 383.4 cm<sup>-1</sup> [60] or to the one (138 N/m) determined from the analysis of dispersion-curves measured by neutron scattering [61]. In the EXAFS study [28], the effective force constant  $\kappa = 204$  N/m for the Mo<sub>0</sub>-S<sub>1</sub> bond was obtained by the conventional EXAFS analysis.

The characteristic Einstein frequency  $\omega_E = 44$  THz is lower for the Mo<sub>0</sub>-Mo<sub>2</sub> atom pairs due to the twice larger value of the respective reduced mass ( $\mu(\text{Mo-O})=24.03$  vs  $\mu(\text{Mo-Mo})=47.97$ ). Nevertheless, the values of the effective force constants  $\kappa = 152$  N/m are equal for the two atom pairs. This fact can be explained by the location of each molybdenum atom at the center

of a trigonal prism composed of six sulfur atoms, while the prisms themselves are connected by edges (Figure 1). Thus, while there is no direct bonding between neighbouring molybdenum atoms, they interact through the two common sulfur atoms at the prism edge. Note that the value of  $\kappa = 137$  N/m was found for the Mo<sub>0</sub>–Mo<sub>2</sub> atom pair in [28].

For atom pairs involving distant atoms (S<sub>4</sub>, S<sub>7</sub>, and Mo<sub>9</sub>) from the nearest neighboring layers, the characteristic Einstein frequencies and the effective force constants have the lowest values suggesting weak interlayer coupling.

The analysis of MSRD factors (Figure 4) indicates significant differences in relative vibrations between atoms in the same layer and the nearest neighboring layers. In general, a linear increase in MSRD values for Mo–S and Mo–Mo atom pairs is expected at higher temperatures due to stronger thermal vibrations [59]. As the separation between two atoms grows, the MSRD value for the pair of atoms should eventually reach a limiting value equal to the sum of their mean-squared displacements, owing to a decrease in the correlation of their motion [62]. Indeed, such behavior was observed in all coordination shells except the ones located in the nearest neighboring layers. The MSRD factors for Mo<sub>0</sub>–S<sub>4</sub>, Mo<sub>0</sub>–S<sub>7</sub>, and Mo<sub>0</sub>–Mo<sub>9</sub> atom pairs are significantly larger than those for other atom pairs at all temperatures. This result suggests that a weak vdW coupling between layers in 2H<sub>c</sub>-MoS<sub>2</sub> leads to highly anisotropic vibrations of Mo and S atoms, being smaller within the layers and larger along the *c*-axis. To summarize, the obtained results demonstrate the sensitivity of EXAFS spectra to such a weak effect as an interlayer coupling in 2DLMs.

To support experimental findings and extend the analysis of lattice dy-



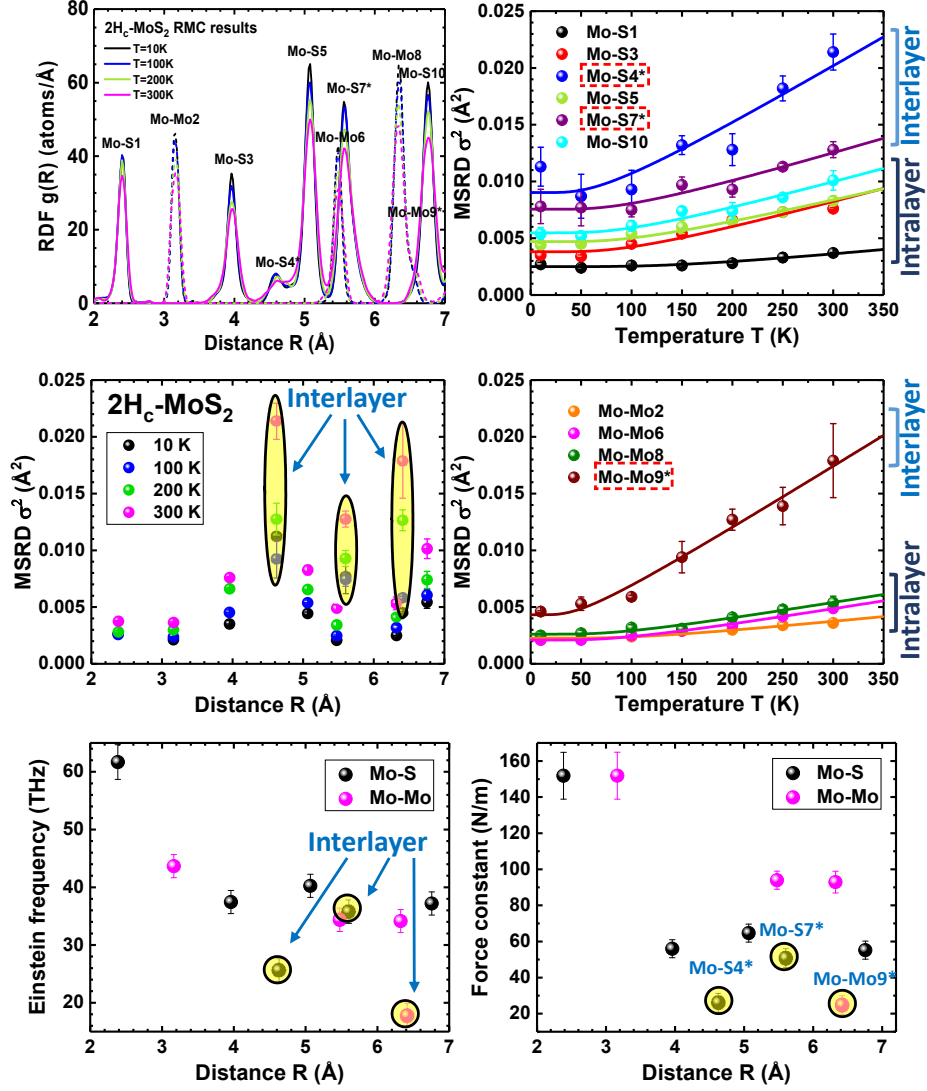


Figure 4: Results of RMC calculations for the Mo K-edge in  $2H_c$ - $\text{MoS}_2$ . Upper left panel: the radial distribution functions for Mo-S and Mo-Mo atom pairs at four temperatures (10 K, 100 K, 200 K, 300 K). Middle left panel: MSRD factors  $\sigma^2(R)$  for Mo-S and Mo-Mo atom pairs as a function of interatomic distance for four temperatures. Upper and middle right panels: temperature dependence of the MSRD factors  $\sigma^2(T)$  for Mo-S and Mo-Mo atom pairs. Lower left and right panels: distance dependence of the characteristic Einstein frequencies  $\omega_E$  and the effective force constants  $\kappa$  for Mo-S and Mo-Mo atom pairs.

namics in  $2H_c$ -MoS<sub>2</sub> to even higher temperatures, ab initio molecular dynamics (AIMD) simulations were performed. The Mo K-edge EXAFS spectrum at 300 K was used to validate the AIMD theory. A comparison between the experimental and AIMD-calculated EXAFS spectra is shown in Figure 5 and suggests good agreement both in  $k$  and  $R$  spaces. The AIMD simulations reproduce well the structure and lattice dynamics in  $2H_c$ -MoS<sub>2</sub> at least up to 7 Å. Note also that the range above the second shell is strongly dominated by the multiple-scattering contributions (blue curves in Figure 5) which, thus, should not be ignored and must be taken into account for accurate analysis.

Being inspired by the results at 300 K, the AIMD simulations were also performed at higher temperatures of 600 K, 900 K, and 1200 K. The MSRD factors for Mo–S and Mo–Mo atom pairs were calculated from atomic coordinates after system equilibration and are shown in Figure 6 for different coordination shells at four temperatures. Note that the MSRD factors for Mo–S atom pairs are slightly larger than those for Mo–Mo atom pairs when close interatomic distances are considered. The results obtained allow us to draw several conclusions. Firstly, upon temperature growth, the absolute values of the MSRD factors increase due to the larger amplitude of atom thermal vibrations. Secondly, at each temperature, the MSRD factors increase up to about 4 Å due to a decrease in the correlation of atomic motion, i.e. due to a reduction of interaction between distant atoms. At the same time, the MSRD values of Mo–S and Mo–Mo atom pairs remain almost unchanged for more distant coordination shells (beyond 4 Å) where the correlation is absent, and the MSRD factors equal to a sum of mean-squared displacements for two atoms. Thirdly, there is a clear difference between the MSRD val-

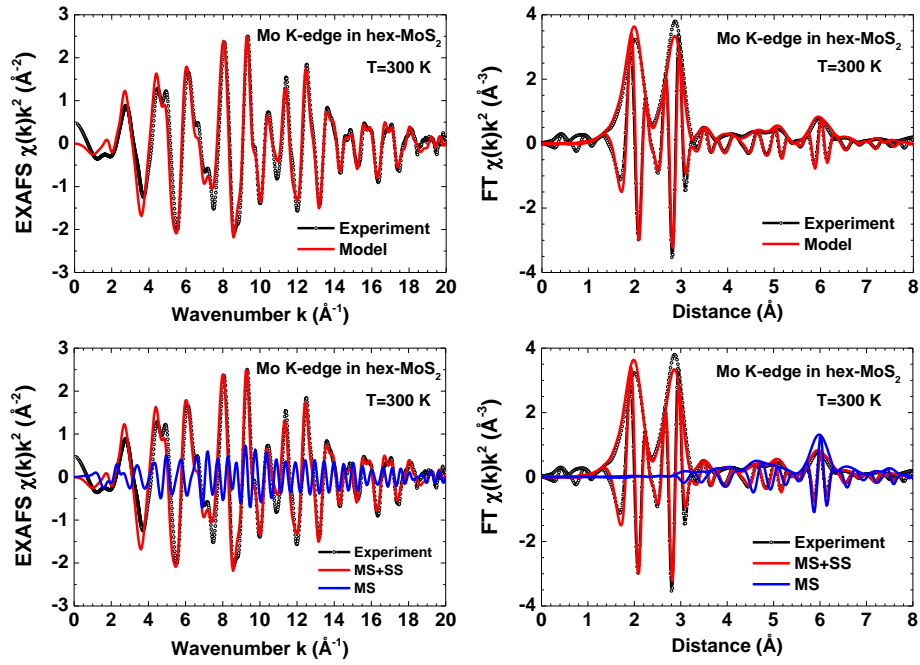


Figure 5: Comparison between the experimental and AIMD calculated Mo K-edge EXAFS spectra  $\chi(k)k^2$  and their Fourier transforms for  $2H_c$ - $\text{MoS}_2$ . The single-scattering and multiple-scattering contributions to the total EXAFS spectrum are shown in the lower panels.

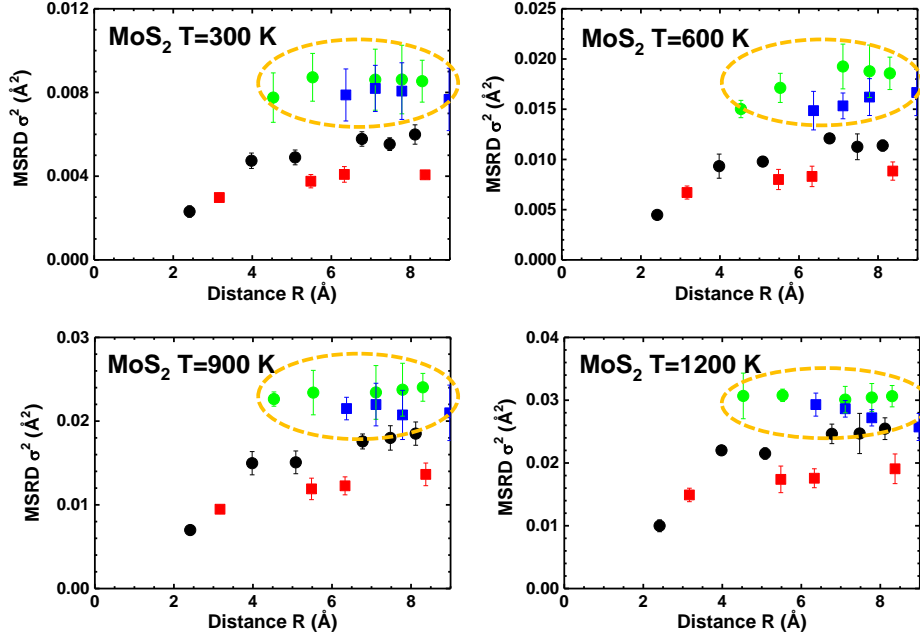


Figure 6: Temperature and interatomic distance dependences of the MSRD factors  $\sigma^2(T)$  for Mo-S (circles) and Mo-Mo (squares) atom pairs obtained from AIMD simulations for 2H<sub>c</sub>-MoS<sub>2</sub>. The MSRD factors for interlayer interactions are indicated by dashed ellipses.

ues for atom pairs within the layer and including atoms from the nearest neighboring layers indicated in Figure 6 by dashed ellipses. The origin of this difference is weak atomic interactions across the vdW gap leading to the anisotropic atomic motion of atoms within the layer and in the orthogonal direction along the  $c$ -axis. Note that strong anisotropy of atom thermal vibrations has been also observed previously by single-crystal X-ray diffraction in 2H- and 3R-MoS<sub>2</sub> polytype phases [55].

## 6. Conclusions

Interlayer and intralayer coupling in two-dimensional layered  $2H_c$ -MoS<sub>2</sub> was studied by the Mo K-edge X-ray absorption spectroscopy and ab initio molecular dynamics (AIMD) simulations. The Mo K-edge EXAFS spectra were measured in the temperature range of 10-300 K, and their analysis using the reverse Monte Carlo (RMC) simulations allowed us to distinguish intralayer and interlayer interactions between absorbing Mo and neighboring S/Mo atoms located within the same or nearby layers, respectively. Temperature dependence of the mean-square relative displacement factors  $\sigma^2$  was determined for the nearest ten coordination shells around molybdenum. The strength of the Mo–S and Mo–Mo interatomic interactions was evaluated in terms of the characteristic Einstein frequencies  $\omega_E$  and the effective force constants  $\kappa$ .

The RMC results obtained at low temperatures were complemented by high-temperature AIMD simulations. The experimental Mo K-edge EXAFS spectrum measured at 300 K was employed to validate the results of the AIMD simulations, which were used to extend the studied temperature range up to 1200 K. Good agreement between the experimental and AIMD calculated EXAFS spectra at 300 K as well as between the mean-square relative displacement factors  $\sigma^2$  for Mo–S and Mo–Mo atom pairs obtained by RMC and AIMD methods proves the reliability of the AIMD simulations.

The AIMD results demonstrate good sensitivity to the temperature dependence of the interatomic interactions and provide evidence of the reduction of correlation in motion between distant atoms. Moreover, both RMC and AIMD results suggest strongly anisotropic vibrational dynamics of atoms

within the plane of the layers and in the orthogonal direction along the  $c$ -axis. The demonstrated methodology opens a new pathway for the investigation of interatomic interactions in layered materials.

### **CRedit authorship contribution statement**

**Inga Pudza:** Investigation, Visualization, Writing – original draft, review & editing. **Dmitry Bocharov:** Conceptualization, Investigation, Writing – original draft, review & editing. **Andris Anspoks:** Investigation. **Matthias Krack:** Methodology, Investigation. **Aleksandr Kalinko:** Investigation. **Edmund Welter:** Resources. **Alexei Kuzmin:** Conceptualization, Investigation, Methodology, Writing – original draft, review & editing.

### **Declaration of Competing Interest**

The authors declare that they have no known competing financial interests or personal relationships that could have appeared to influence the work reported in this paper.

### **Acknowledgements**

D.B. and A.K. thank the support of the Latvian Council of Science project No. LZP-2020/1-0261. The experiment at the PETRA III synchrotron was performed within proposal No. I-20170739 EC. The synchrotron experiment has been supported by the project CALIPSOplus under the Grant Agreement 730872 from the EU Framework Programme for Research and Innovation HORIZON 2020. We acknowledge that the results of AIMD simulations

have been achieved using the DECI resource Beskow based in Sweden at KTH Royal Institute of Technology in Stockholm with support from the PRACE (DECI15 project WS2MoS2AIMD). The technical support of Lilit Axner is gratefully acknowledged. Institute of Solid State Physics, University of Latvia as the Center of Excellence has received funding from the European Union's Horizon 2020 Framework Programme H2020-WIDESPREAD-01-2016-2017-TeamingPhase2 under grant agreement No. 739508, project CAMART2.

#### **Data availability statement**

Data will be made available on request.

## References

- [1] A. Gupta, T. Sakthivel, S. Seal, Recent development in 2D materials beyond graphene, *Prog. Mater. Sci.* 73 (2015) 44–126. doi:10.1016/j.pmatsci.2015.02.002.
- [2] V. K. Sangwan, S. E. Liu, A. R. Trivedi, M. C. Hersam, Two-dimensional materials for bio-realistic neuronal computing networks, *Matter* 5 (2022) 4133–4152. doi:10.1016/j.matt.2022.10.017.
- [3] K. S. Novoselov, A. Mishchenko, A. Carvalho, A. H. Castro Neto, 2D materials and van der Waals heterostructures, *Science* 353 (2016) aac9439. doi:10.1126/science.aac9439.
- [4] P. Kumar, H. Abuhimd, W. Wahyudi, M. Li, J. Ming, L.-J. Li, Review—two-dimensional layered materials for energy storage applications, *ECS J. Solid State Sci. Technol.* 5 (2016) Q3021. doi:10.1149/2.0051611jss.
- [5] H. Zhan, D. Guo, G. Xie, Two-dimensional layered materials: from mechanical and coupling properties towards applications in electronics, *Nanoscale* 11 (2019) 13181–13212. doi:10.1039/C9NR03611C.
- [6] H. R. Gutiérrez, Two-dimensional layered materials offering expanded applications in flatland, *ACS Appl. Nano Mater.* 3 (2020) 6134–6139. doi:10.1021/acsanm.0c01763.
- [7] S. Kaushik, R. Singh, 2D layered materials for ultraviolet photodetection: A review, *Adv. Opt. Mater.* 9 (2021) 2002214. doi:10.1002/adom.202002214.



- [8] M. Lanza, I. Radu, Electronic circuits made of 2D materials, *Adv. Mater.* 34 (2022) 2207843. doi:10.1002/adma.202207843.
- [9] A. T. Hoang, L. Hu, A. K. Katiyar, J.-H. Ahn, Two-dimensional layered materials and heterostructures for flexible electronics, *Matter* 5 (2022) 4116–4132. doi:10.1016/j.matt.2022.10.016.
- [10] V. Shanmugam, R. A. Mensah, K. Babu, S. Gawusu, A. Chanda, Y. Tu, R. E. Neisiany, M. Försth, G. Sas, O. Das, A review of the synthesis, properties, and applications of 2D materials, *Part. Part. Syst. Charact.* 39 (2022) 2200031. doi:10.1002/ppsc.202200031.
- [11] Y. Liu, N. Weiss, X. Duan, H.-C. Cheng, Y. Huang, X. Duan, Van der Waals heterostructures and devices, *Nat. Rev. Mater.* 1 (2016) 16042. doi:10.1038/natrevmats.2016.42.
- [12] Z. Shi, X. Wang, Y. Sun, Y. Li, L. Zhang, Interlayer coupling in two-dimensional semiconductor materials, *Semicond. Sci. Technol.* 33 (2018) 093001. doi:10.1088/1361-6641/aad6c3.
- [13] R. Bian, C. Li, Q. Liu, G. Cao, Q. Fu, P. Meng, J. Zhou, F. Liu, Z. Liu, Recent progress in the synthesis of novel two-dimensional van der Waals materials, *Natl. Sci. Rev.* 9 (2021) nwab164. doi:10.1093/nsr/nwab164.
- [14] Y. Pak, W. Park, S. Mitra, A. A. Sasikala Devi, K. Loganathan, Y. Kumaresan, Y. Kim, B. Cho, G.-Y. Jung, M. M. Hussain, I. S. Roqan, Enhanced performance of MoS<sub>2</sub> photodetectors by inserting

- an ALD-processed TiO<sub>2</sub> interlayer, *Small* 14 (2018) 1703176. doi:10.1002/smll.201703176.
- [15] G.-H. Lee, X. Cui, Y. D. Kim, G. Arefe, X. Zhang, C.-H. Lee, F. Ye, K. Watanabe, T. Taniguchi, P. Kim, J. Hone, Highly stable, dual-gated MoS<sub>2</sub> transistors encapsulated by hexagonal boron nitride with gate-controllable contact, resistance, and threshold voltage, *ACS Nano* 9 (2015) 7019–7026. doi:10.1021/acsnano.5b01341.
- [16] W. Li, J. Zhou, S. Cai, Z. Yu, J. Zhang, N. Fang, T. Li, Y. Wu, T. Chen, X. Xie, H. Ma, K. Yan, N. Dai, X. Wu, H. Zhao, Z. Wang, D. He, L. Pan, Y. Shi, P. Wang, W. Chen, K. Nagashio, X. Duan, X. Wang, Uniform and ultrathin high- $\kappa$  gate dielectrics for two-dimensional electronic devices, *Nat. Electron.* 2 (2019) 563–571. doi:10.1038/s41928-019-0334-y.
- [17] S. Das, A. Sebastian, E. Pop, C. J. McClellan, A. D. Franklin, T. Grasser, T. Knobloch, Y. Illarionov, A. V. Penumatcha, J. Appenzeller, Z. Chen, W. Zhu, I. Asselberghs, L.-J. Li, U. E. Avci, N. Bhat, T. D. Anthopoulos, R. Singh, Transistors based on two-dimensional materials for future integrated circuits, *Nat. Electron.* 4 (2021) 786–799. doi:10.1038/s41928-021-00670-1.
- [18] S. B. Desai, S. R. Madhvapathy, A. B. Sachid, J. P. Llinas, Q. Wang, G. H. Ahn, G. Pitner, M. J. Kim, J. Bokor, C. Hu, H.-S. P. Wong, A. Javey, MoS<sub>2</sub> transistors with 1-nanometer gate lengths, *Science* 354 (6308) (2016) 99–102. doi:10.1126/science.aah4698.

- [19] S. Wachter, D. K. Polyushkin, O. Bethge, T. Mueller, A microprocessor based on a two-dimensional semiconductor, *Nat. Commun.* 8 (2017) 14948. doi:10.1038/ncomms14948.
- [20] G. Migliato Marega, Y. Zhao, A. Avsar, Z. Wang, M. Tripathi, A. Radenovic, A. Kis, Logic-in-memory based on an atomically thin semiconductor, *Nature* 587 (2020) 72–77. doi:10.1038/s41586-020-2861-0.
- [21] A. C. Ferrari, F. Bonaccorso, V. Fal’ko, K. S. Novoselov, S. Roche, P. Boggild, S. Borini, F. H. L. Koppens, V. Palermo, N. Pugno, J. A. Garrido, R. Sordan, A. Bianco, L. Ballerini, M. Prato, E. Lidorikis, J. Kivioja, C. Marinelli, T. Ryhanen, A. Morpurgo, J. N. Coleman, V. Nicolosi, L. Colombo, A. Fert, M. Garcia-Hernandez, A. Bachtold, G. F. Schneider, F. Guinea, C. Dekker, M. Barbone, Z. Sun, C. Galiotis, A. N. Grigorenko, G. Konstantatos, A. Kis, M. Katsnelson, L. Vandersypen, A. Loiseau, V. Morandi, D. Neumaier, E. Treossi, V. Pellegrini, M. Polini, A. Tredicucci, G. M. Williams, B. Hee Hong, J.-H. Ahn, J. Min Kim, H. Zirath, B. J. van Wees, H. van der Zant, L. Occhipinti, A. Di Matteo, I. A. Kinloch, T. Seyller, E. Quesnel, X. Feng, K. Teo, N. Rupesinghe, P. Hakonen, S. R. T. Neil, Q. Tannock, T. Lofwander, J. Kinaret, Science and technology roadmap for graphene, related two-dimensional crystals, and hybrid systems, *Nanoscale* 7 (2015) 4598–4810. doi:10.1039/C4NR01600A.
- [22] X. Li, L. Tao, Z. Chen, H. Fang, X. Li, X. Wang, J.-B. Xu, H. Zhu, Graphene and related two-dimensional materials: Structure-property re-

- lationships for electronics and optoelectronics, *Appl. Phys. Rev.* 4 (2017) 021306. doi:10.1063/1.4983646.
- [23] E. Butanovs, S. Vlassov, A. Kuzmin, S. Piskunov, J. Butikova, B. Polyakov, Fast-response single-nanowire photodetector based on ZnO/WS<sub>2</sub> core/shell heterostructures, *ACS Appl. Mater. Interfaces* 10 (2018) 13869–13876. doi:10.1021/acsami.8b02241.
- [24] B. Polyakov, A. Kuzmin, K. Smits, J. Zideluns, E. Butanovs, J. Butikova, S. Vlassov, S. Piskunov, Y. F. Zhukovskii, Unexpected epitaxial growth of a few WS<sub>2</sub> layers on {1 $\bar{1}$ 00} facets of ZnO nanowires, *J. Phys. Chem. C* 120 (2016) 21451–21459. doi:10.1021/acs.jpcc.6b06139.
- [25] S. J. L. Billinge, I. Levin, The problem with determining atomic structure at the nanoscale, *Science* 316 (2005) 561–565. doi:10.1126/science.1135080.
- [26] M. Stöhr, T. Van Voorhis, A. Tkatchenko, Theory and practice of modeling van der Waals interactions in electronic-structure calculations, *Chem. Soc. Rev.* 48 (2019) 4118–4154. doi:10.1039/C9CS00060G.
- [27] D. Y. Chung, S.-K. Park, Y.-H. Chung, S.-H. Yu, D.-H. Lim, N. Jung, H. C. Ham, H.-Y. Park, Y. Piao, S. J. Yoo, Y.-E. Sung, Edge-exposed MoS<sub>2</sub> nano-assembled structures as efficient electrocatalysts for hydrogen evolution reaction, *Nanoscale* 6 (2014) 2131–2136. doi:10.1039/C3NR05228A.
- [28] S. Caramazza, C. Marini, L. Simonelli, P. Dore, P. Postorino, Temperature dependent EXAFS study on transition metal dichalcogenides

- MoX<sub>2</sub> (X = S, Se, Te), *J. Phys.: Condens. Matter* 28 (2016) 325401. doi:10.1088/0953-8984/28/32/325401.
- [29] D. A. Kuznetsov, Z. Chen, P. V. Kumar, A. Tsoukalou, A. Kierzkowska, P. M. Abdala, O. V. Safonova, A. Fedorov, C. R. Muller, Single site cobalt substitution in 2D molybdenum carbide (MXene) enhances catalytic activity in the hydrogen evolution reaction, *J. Am. Chem. Soc.* 141 (2019) 17809–17816. doi:10.1021/jacs.9b08897.
- [30] A. Kuzmin, J. Chaboy, EXAFS and XANES analysis of oxides at the nanoscale, *IUCrJ* 1 (2014) 571–589. doi:10.1107/S2052252514021101.
- [31] A. Kuzmin, J. Timoshenko, A. Kalinko, I. Jonane, A. Anspoks, Treatment of disorder effects in X-ray absorption spectra beyond the conventional approach, *Rad. Phys. Chem.* 175 (2020) 108112. doi:10.1016/j.radphyschem.2018.12.032.
- [32] J. J. Rehr, R. C. Albers, Theoretical approaches to x-ray absorption fine structure, *Rev. Mod. Phys.* 72 (2000) 621–654. doi:10.1103/RevModPhys.72.621.
- [33] P. Joensen, E. D. Crozier, N. Alberding, R. F. Frindt, A study of single-layer and restacked MoS<sub>2</sub> by X-ray diffraction and X-ray absorption spectroscopy, *J. Phys. C: Solid State Physics* 20 (1987) 4043. doi:10.1088/0022-3719/20/26/009.
- [34] O. Belyakova, Y. Zubavichus, I. Neretin, A. Golub, Y. Novikov, E. Mednikov, M. Vargaftik, I. Moiseev, Y. Slovokhotov, Atomic structure of

- nanomaterials: combined X-ray diffraction and EXAFS studies, *J. Alloys Compd.* 382 (2004) 46–53. doi:10.1016/j.jallcom.2004.05.047.
- [35] B. Lassalle-Kaiser, D. Merki, H. Vrubel, S. Gul, V. K. Yachandra, X. Hu, J. Yano, Evidence from in situ X-ray absorption spectroscopy for the involvement of terminal disulfide in the reduction of protons by an amorphous molybdenum sulfide electrocatalyst, *J. Am. Chem. Soc.* 137 (2015) 314–321. doi:10.1021/ja510328m.
- [36] H. P. Zhang, H. F. Lin, Y. Zheng, Y. F. Hu, A. MacLennan, The catalytic activity and chemical structure of nano MoS<sub>2</sub> synthesized in a controlled environment, *React. Chem. Eng.* 1 (2016) 165–175. doi:10.1039/C5RE00046G.
- [37] S.-H. Kim, K.-D. Kim, Y.-K. Lee, Effects of dispersed MoS<sub>2</sub> catalysts and reaction conditions on slurry phase hydrocracking of vacuum residue, *J. Catal.* 347 (2017) 127–137. doi:10.1016/j.jcat.2016.11.015.
- [38] E. Welter, R. Chernikov, M. Herrmann, R. Nemausat, A beamline for bulk sample x-ray absorption spectroscopy at the high brilliance storage ring PETRA III, *AIP Conf. Proc.* 2054 (2019) 040002. doi:10.1063/1.5084603.
- [39] J. Timoshenko, A. Kuzmin, J. Purans, Reverse Monte Carlo modeling of thermal disorder in crystalline materials from EXAFS spectra, *Comp. Phys. Commun.* 183 (2012) 1237–1245. doi:10.1016/j.cpc.2012.02.002.

- [40] J. Timoshenko, A. Kuzmin, J. Purans, EXAFS study of hydrogen intercalation into  $\text{ReO}_3$  using the evolutionary algorithm, *J. Phys.: Condens. Matter* 26 (2014) 055401. doi:10.1088/0953-8984/26/5/055401.
- [41] R. W. G. Wyckoff, *Crystal Structures*, Vol. 1, Interscience Publishers, New York, 1963.
- [42] A. L. Ankudinov, B. Ravel, J. J. Rehr, S. D. Conradson, Real-space multiple-scattering calculation and interpretation of x-ray-absorption near-edge structure, *Phys. Rev. B* 58 (1998) 7565–7576. doi:10.1103/PhysRevB.58.7565.
- [43] L. Hedin, B. I. Lundqvist, Explicit local exchange-correlation potentials, *J. Phys. C: Solid State Phys.* 4 (1971) 2064. doi:10.1088/0022-3719/4/14/022.
- [44] J. Timoshenko, A. Kuzmin, Wavelet data analysis of EXAFS spectra, *Comp. Phys. Commun.* 180 (2009) 920–925. doi:10.1016/j.cpc.2008.12.020.
- [45] F. R. Hampel, Robust estimation: A condensed partial survey, *Z. Wahrscheinlichkeit.* 27 (1973) 87–104. doi:10.1007/BF00536619.
- [46] M. Daszykowski, K. Kaczmarek, Y. Vander Heyden, B. Walczak, Robust statistics in data analysis—A review: Basic concepts, *Chemom. Intell. Lab. Syst.* 85 (2007) 203–219. doi:10.1016/j.chemolab.2006.06.016.
- [47] W. Kohn, L. J. Sham, Self-consistent equations including exchange and correlation effects, *Phys. Rev.* 140 (1965) A1133–A1138. doi:10.1103/PhysRev.140.A1133.

- [48] T. D. Kuhne, M. Iannuzzi, M. D. Ben, V. V. Rybkin, P. Seewald, F. Stein, T. Laino, R. Z. Khaliullin, O. Schutt, F. Schiffmann, D. Golze, J. Wilhelm, S. Chulkov, M. H. Bani-Hashemian, V. Weber, U. Borštnik, M. TAILLEFUMIER, A. S. Jakobovits, A. Lazzaro, H. Pabst, T. Muller, R. Schade, M. Guidon, S. Andermatt, N. Holmberg, G. K. Schenter, A. Hehn, A. Bussy, F. Belleflamme, G. Tabacchi, A. Gloß, M. Lass, I. Bethune, C. J. Mundy, C. Plessl, M. Watkins, J. VandeVondele, M. Krack, J. Hutter, CP2K: An electronic structure and molecular dynamics software package – Quickstep: Efficient and accurate electronic structure calculations, *J. Chem. Phys.* 152 (2020) 194103. doi: 10.1063/5.0007045.
- [49] J. VandeVondele, M. Krack, F. Mohamed, M. Parrinello, T. Chassaing, J. Hutter, Quickstep: Fast and accurate density functional calculations using a mixed Gaussian and plane waves approach, *Comp. Phys. Commun.* 167 (2005) 103–128.
- [50] G. Lippert, J. Hutter, M. Parrinello, A hybrid Gaussian and plane wave density functional scheme, *Mol. Phys.* 92 (1997) 477.
- [51] J. P. Perdew, K. Burke, M. Ernzerhof, Generalized gradient approximation made simple, *Phys. Rev. Lett.* 77 (1996) 3865–3868. doi: 10.1103/PhysRevLett.77.3865.
- [52] S. Grimme, J. Antony, S. Ehrlich, H. Krieg, A consistent and accurate ab initio parametrization of density functional dispersion correction (DFT-D) for the 94 elements H-Pu, *J. Chem. Phys.* 132 (2010) 154104. doi: 10.1063/1.3382344.



- [53] G. Bussi, D. Donadio, M. Parrinello, Canonical sampling through velocity rescaling, *J. Chem. Phys.* 126 (2007) 014101. doi:10.1063/1.2408420.
- [54] A. Kuzmin, R. A. Evarestov, Quantum mechanics–molecular dynamics approach to the interpretation of x-ray absorption spectra, *J. Phys.: Condens. Matter* 21 (2009) 055401. doi:10.1088/0953-8984/21/5/055401.
- [55] B. Schönfeld, J. J. Huang, S. C. Moss, Anisotropic mean-square displacements (MSD) in single-crystals of 2H- and 3R-MoS<sub>2</sub>, *Acta Cryst. B* 39 (1983) 404–407. doi:10.1107/S0108768183002645.
- [56] I. Jonane, A. Anspoks, A. Kuzmin, Advanced approach to the local structure reconstruction and theory validation on the example of the W L<sub>3</sub>-edge extended x-ray absorption fine structure of tungsten, *Modelling Simul. Mater. Sci. Eng.* 26 (2018) 025004. doi:10.1088/1361-651x/aa9bab.
- [57] G. Bakradze, A. Kalinko, A. Kuzmin, Evidence of nickel ions dimerization in NiWO<sub>4</sub> and NiWO<sub>4</sub>-ZnWO<sub>4</sub> solid solutions probed by EXAFS spectroscopy and reverse Monte Carlo simulations, *Acta Mater.* 217 (2021) 117171. doi:10.1016/j.actamat.2021.117171.
- [58] E. A. Kotomin, A. Kuzmin, J. Purans, J. Timoshenko, S. Piskunov, R. Merkle, J. Maier, Theoretical and experimental studies of charge ordering in CaFeO<sub>3</sub> and SrFeO<sub>3</sub> crystals, *Phys. Status Solidi B* 259 (2022) 2100238. doi:10.1002/pssb.202100238.

- [59] E. Sevillano, H. Meuth, J. Rehr, Extended x-ray absorption fine structure Debye-Waller factors. I. Monatomic crystals, *Phys. Rev. B* 20 (1979) 4908. doi:10.1103/PhysRevB.20.4908.
- [60] A. Bagnall, W. Liang, E. Marseglia, B. Welber, Raman studies of MoS<sub>2</sub> at high pressure, *Physica B+C* 99 (1980) 343–346. doi:10.1016/0378-4363(80)90257-0.
- [61] N. Wakabayashi, H. G. Smith, R. M. Nicklow, Lattice dynamics of hexagonal MoS<sub>2</sub> studied by neutron scattering, *Phys. Rev. B* 12 (1975) 659–663. doi:10.1103/PhysRevB.12.659.
- [62] I.-K. Jeong, R. H. Heffner, M. J. Graf, S. J. L. Billinge, Lattice dynamics and correlated atomic motion from the atomic pair distribution function, *Phys. Rev. B* 67 (2003) 104301. doi:10.1103/PhysRevB.67.104301.